1979A&AS...36..173H

1979, *Astron. Astrophys. Suppl.* **36**, 173-192.

A STUDY OF THE RADIO GALAXIES 3C111, 192, 219, 223, 315 AND 452

J.A. HÖGBOM
Stockholm Observatory, Sweden

Received June 28, 1978

The Westerbork synthesis telescope has been used to observe the radio galaxies 3C111, 192, 219, 223, 315 and 452 at 4995 MHz. The sources were selected for their prominent tail-bridge radio components. The new measurements are used in conjunction with earlier measurements at 1415 MHz to derive the distribution over these sources of spectral index, rotation measure and depolarization as well as the projected magnetic field configuration.

All six sources contain a central unresolved radio component coincident with the optical object. In 3C219 and probably also in 3C315 there is a polarized jet associated with the central component.

There is clear evidence for variations in spectral index, rotation measure and/or depolarization over individual radio lobes. The spectrum gets progressively steeper towards the central regions of 3C219, 3C223 and 3C452. The spectral data is used to derive values of physical parameters in the extended regions of emission. It also leads to estimates of the velocity of the heads and of the ages of the sources.

Tails and bridges as well as some of the structure in the bright heads are typically 10-30% linearly polarized. The polarization in some special areas, however, can approach 50%. Most sources show little depolarization between 4995 and 1415 MHz. 2695 MHz polarization measurements by Fomalont (private communication) were used to solve problems connected with rotation measure ambiguities. The rotation measure in the heads of these sources is not greatly different from that of adjacent polarized regions.

The projected magnetic field configuration is clearly related to details in the total intensity distribution. With very few exceptions the field runs parallel to boundaries and other elongated features. A comparison with published high resolution maps of the radio heads shows this relation to hold also here. It is suggested that the three-dimensional configuration of the magnetic field is basically irregular and that polarized emission is observed from regions in which shear and/or compression has made the field anisotropic.

Key words: radio galaxies – radio polarization – magnetic fields – intergalactic medium

1. INTRODUCTION

Theoretical work on extragalactic radio sources in recent years has focussed on models based on the streaming of relativistic particles and/or hot plasma from the nucleus of the parent galaxy. According to these models shock fronts are formed where such streams collide with the intergalactic medium. A reservoir containing relativistic particles and magnetic fields is built up in the wake of the advancing shock. This reservoir is thought to be responsible for the "tails" and "bridges" of emission which are observed in many sources (Scheuer 1974, De Young 1977). In this paper I discuss multi-frequency observations of six sources, the tails and bridges of which are unusually bright and well defined. They are all identified with galaxies whose redshifts have been measured (table I).

The observations and the data reduction are described in section 2. Section 3 contains a morphological description of the sources. Spectral index data are presented in section 4 together with the energy densities and magnetic field intensities calculated for selected locations in the extended emission regions. Sections 5 and 6 are concerned with the magnetic field configuration throughout the sources while rotation measure and depolarization results are presented in section 7.

2. OBSERVATIONS AND DATA REDUCTION

Each source was observed at 4995 MHz for one 12-hour period with the Westerbork synthesis telescope (Högbom and Brouw 1974, Weiler 1973). 20 interferometers were used covering the spacings between 54 and 1422 metres at regular intervals of 72 metres. The r.m.s. noise level on the maps is about 1 mJy and the angular resolution corresponds to a $7.0 \times 7.0/\sin \delta$ arcsec synthesized beam. The full reception pattern contains a set of grating rings, the closest of which has a radius of 2.8 and $2.8/\sin \delta$ arcmin in the right ascension and declination directions respectively. The rings cause disturbances to the synthesized maps,

© European Southern Observatory • Provided by the NASA Astrophysics Data System

1979A&AS...36..173H

because the sources are comparable in angular size to the radius of the closest ring. The influence of the rings was therefore eliminated by the procedure CLEAN (Högbom 1974).

Contour maps of the total intensity and the linearly polarized intensity for the six sources are shown in figure 1. A cross shows the optical position of the parent galaxy. The direction of the electric vector is indicated by the short lines on the polarization maps and the half power contour of the synthesized beam is shown in one corner of the total intensity maps. The contour interval expressed in mJy is given with each map; a point source with this flux density will cause a peak deflection of one contour interval. A dashed contour, when present, indicates the level of one half contour interval. Zero contours, as well as the occasional negative contour on the total intensity maps, have been suppressed for clarity. Over extended areas, one contour interval of ΔS mJy corresponds to a brightness temperature interval of $\Delta T_B = 1.28 \cdot \Delta S \cdot \sin \delta$ K.

The new measurements were compared with earlier 1415 MHz measurements of the same sources (Högbom and Carlsson 1974). For this purpose, the original 4995 MHz maps were smoothed to a $12 \times 12/\sin \delta$ arcsec resolution, cleaned at this resolution and then further smoothed to a resolution corresponding to a $22 \times 22/\sin \delta$ arcsec gaussian beam. The pre-smoothing improves the signal/noise over extended emission regions, the grating responses of which can then be more effectively removed by the clean process. New maps with the same gaussian beam were prepared from the original 1415 MHz interferometer measurements again using the CLEAN algoritm.

The *(u, v)* interferometer spacing domain was sampled in a different way at the two frequencies. The CLEAN algoritm attempts to reconstruct that map which would have been obtained if the *(u, v)* plane had been sampled in a uniform manner. If this succeeds, the low resolution maps described above will have identical *(u, v)* coverage and can be compared directly. The procedure fails if at some frequency the sampling is insufficient to define the source structure with the required accuracy. This does not seem to be a problem with the present measurements. A special difficulty is that the shortest spacing (54 m) does not permit satisfactory recording at 4995 MHz of smooth extended components which are 2 arcmin or more in both dimensions. However, with the exception of 3C111, no structures of such dimensions are seen on the 1415 MHz maps where they ought to be clearly visible.

When the rotation measure distribution over a source is known, the observed polarization position angle can be corrected for the Faraday rotation. The direction perpendicular to the corrected polarization position angle will be referred to as the direction of the projected magnetic field and we shall later discuss to what extent this is representative of the actual magnetic field geometry in the sources.

Good integrated rotation measures are available for 3C111, 192, 315 and 452 (Haves 1975). High resolution polarization observations of all sources except 3C192 have been made by Fomalont at 2695 MHz (private communication). The correct rotation measure at any point in a source was taken to be the (absolute) lowest value from the low resolution 1415/4995 MHz comparison which was also compatible with the integrated value and/or the 2695 MHz map. The exception was 3C452, for which the observations are compatible not only with the value listed by Haves (-272 rad m^{-2}) but also with a lower absolute value of the order of $+80$ rad m^{-2}. The former value was accepted for the following reasons: a) the paper by Haves, b) a detailed comparison of the position angles at all three frequencies favoured this value, and c) the direction of the derived projected magnetic field would change by about 75° if the lower value were chosen, making the field geometry quite artificial (see figure 4). This last argument may in fact be used as an *a posteriori* confirmation of the accepted *RM* alternative for all the sources.

The low to moderate depolarization between 4995 and 1415 MHz in most sources indicates that large variations of the rotation measure on an angular scale much smaller than the $22 \times 22/\sin \delta$ arcsec beam are unlikely. The rotation measure distributions from the low resolution two frequency comparisons were therefore used to correct the full resolution 4995 MHz maps for Faraday rotation and so arrive at the projected magnetic field configuration. The field in some weak extended areas was determined from the $12 \times 12/\sin \delta$ arcsec resolution maps described earlier. The interpretation of complex regions close to the heads is discussed in section 5.

© European Southern Observatory • Provided by the NASA Astrophysics Data System

1979A&AS...36..173H

3. THE TOTAL INTENSITY DISTRIBUTIONS

All sources except 3C315 display the characteristic elongated structure, usually with "hot spots" at or near the extreme edges. They all have a central unresolved radio component coincident with the optical object. The radio structure in the central parts of 3C192 is confused, but the detailed shape of the contours close to the position of the parent galaxy clearly indicates the presence of a weak unresolved central component. The 4995 MHz flux densities and positions produced by a point source searching computer programme are given in table I. The 1415 MHz flux densities derive from a detailed comparison of the $22 \times 22/\sin \delta$ arcsec resolution maps at the two frequencies.

The radio jet associated with the central component of 3C219 has been previously discussed by Turland (1975). A similar structure is seen in p.a. 12° of the intense central component of 3C315. The position angle agrees with that of the central compact component which has been resolved by the Cambridge 5 km telescope (Northover 1976) as well as with that of the well defined outer Nf-Sp extensions.

The "normal" lobe structure with a leading small diameter bright head containing one or more "hot spots" followed by a tail with progressively decreasing brightness is seen in 3C111 Nf component, the 3C223 Np component and in both components of 3C219 and 3C452. Both hot spots in 3C219 are far from the outer edge of their corresponding lobe. A line drawn through the nuclear source and the jet cuts the Sp hot spot and also passes the extreme outer edge of this lobe. It is remarkable that the same line completely misses the Nf hot spot while it does in fact go through the extreme outer edge where one would normally expect the hot spot to be situated.

All bright heads in the present sample, with the possible exception of that in the 3C111 Nf lobe, are complex in nature. Most of these regions have been mapped in detail with the Cambridge 5 km telescope (Jenkins *et al.* 1977, Riley and Pooley 1975, Turland 1975, see figure 5). On the relativistic beam model the complex head structure may be understood as a consequence of variations in beam direction and intensity.

The sources had been selected for their prominent tail/bridge components. Most of these structures are well resolved at 4995 MHz, also in a direction perpendicular to their axes. Profiles of tails and bridges taken perpendicular to their axes vary in detail but are usually in reasonable agreement with those expected from a model with uniform emission from within a circularly cylindrical source. Deviations from this simple model are not in general such as to suggest a systematic limb brightening or limb darkening. They are probably a consequence of the complex structure in the associated head. The 3C223 Np lobe appears to give double humped profiles suggestive of a cylindrical shell source. A detailed comparison with the expected profiles shows this to be illusory; there are substantial deviations from both models, but the uniform emission model still gives a somewhat better fit.

Within the framework of the model calculations by De Young (1977), these results support his conclusion that the dynamics of the extended emission regions is dominated not by relativistic particles and magnetic fields but by thermal plasma. There is indeed a remarkable qualitative similarity between his figure 5a and the structure of the best resolved source in the present sample, 3C452 (figure 1). His calculations are based on a model with a spherically symmetrical active region moving through an intergalactic medium. Rayburn (1977) has made similar calculations on a relativistic beam model with no mixed in thermal plasma. His results confirm those of De Young in that such a situation is expected to produce limb brightening which is not observed.

Deviations from linear symmetry are commonly seen in extragalactic radio sources. Many types of deviation, e.g. those observed in the low level radiation from 3C111 (figure 2), are most likely due to the drag forces of an intergalactic medium which is not at rest relative to the parent galaxy (Miley *et al.* 1972, Harris 1974). The remarkable rotational symmetries in 3C192, 3C315 and 3C452 are different in nature. Whatever the true reason for these distorsions, however, the many qualitative similarities between 3C192 and 3C315, which are also obvious in their magnetic field configurations, suggest that we are observing basically the same phenomenon in these two sources. If the hot spots in 3C192 were to fade, then, apart from a weaker

© European Southern Observatory • Provided by the NASA Astrophysics Data System

1979A&AS...36..173H

central compact component, this source would not be unlike 3C315. Thus, 3C315 should not be regarded as a fundamentally different type of source. A physically meaningful axis is probably at present running in the direction defined by the shape of the central component referred to above and by the Nf and Sp extensions. Profiles across these extensions are good fits to the uniform cylinder emission model while profiles across the Sf extension are not. The Np extension is too weak for a meaningful comparison. The observed rotation symmetrical deviations in these sources are compatible with the existence of a precessing "power-house" at the nucleus of the parent galaxy (Miley 1976).

4. SPECTRAL INDEX DISTRIBUTION OVER THE SOURCES

A comparison of the $22 \times 22/\sin \delta$ arcsec resolution maps at 1415 and 4995 MHz shows that there are significant variations of the spectral index over some sources. Profiles through these maps of the total intensity, spectral index, degree of polarization and rotation measure are displayed in figure 3. Each profile runs along two connecting straight lines. The first goes through the E outer maximum to the central unresolved component and the second continues from there through the W outer maximum.

Central unresolved components, as expected, have flatter spectra than other parts of the sources. Dashed lines in the profiles, when present, refer to the shape of the profiles after subtracting the contribution from the central component (table I). Only upper limits to the 1415 MHz flux could be determined for 3C192, 219 and 223, and here a point source with a nominal flux density equal to that at 4995 MHz was subtracted. The brightness distributions of the sources are such that the conclusions are not very sensitive to the exact value of the 1415 MHz flux density of the central component.

Large differences in spectral index exist in the main radio lobes of 3C219, 223 and 452. The spectra become progressively steeper towards the inner parts of these sources. The measurements of 3C452 are in good agreement with those of Burch (1977). He also showed that the steep spectra in this source cannot continue far towards lower frequencies since this would conflict with available low frequency measurements. A minor malfunctioning of the telescope during the 4995 MHz measurements of 3C111 makes it difficult to get reliable values of the spectral index in the faint extended emission regions of this source, but there is some evidence for a similar, but less marked, gradual steepening of the spectrum in the Nf lobe. The low level emission region towards the NW (figure 2) is clearly present on the corresponding low resolution 4995 MHz map. Its spectrum cannot be much steeper than that over the rest of the source.

The four sources discussed so far have radio tail structures, the brightness of which falls off gradually with the distance from the outer edge of the respective lobe. The detailed structure of 3C219 is complicated, but the extended emission regions still appear to retain much of their original spectral characteristics. The two remaining sources 3C192 and 3C315 are different in character. The extended emission regions cannot be described as simple tails with gradually decreasing brightness and the spectral index distribution is nearly uniform. The low brightness "wing" portions of 3C192 as well as the weak Np extension of 3C315 appear to have steeper spectra than the main portions of these sources.

Table II contains values of some relevant parameters calculated for two or three representative locations in each source. The selected locations are marked on the maps of figure 1. The calculations were made assuming that a) relativistic electrons and protons with equal energy density are generated with a power law energy spectrum corresponding to the radio spectral index α_h (1415, 4995) measured in and near the head of the same radio lobe, b) the observed steepening of the spectra is due to energy losses by synchrotron emission and by inverse Compton encounters with photons of the universal microwave radiation and c) there has been no significant mixing of electrons of different age. We shall return to this last point in section 6.

With these assumptions, the three quantities B (4995), α (1415, 4995) and α_h (1415, 4995) define the complete radio spectrum as well as the electron energy spectrum including the electron cut off energy. The u_{min} values were computed for electrons radiating in the frequency range 10 MHz – 10 GHz; the exact choice of upper frequency limit makes little difference in practice. The lower frequency limit, however,

© European Southern Observatory • Provided by the NASA Astrophysics Data System

1979A&AS...36..173H

is more important. If the power law spectrum at the selected locations were to continue at much lower frequencies, about which we have no direct information, then this would raise the values of $u_{\min}$ and $H_{\rm eq}$.

The electron age $t_{\rm eq}$ is computed from the spectral data assuming an equipartition field $H_{\rm eq}$. The absolute upper limit to the electron age is obtained for a field $H_{\rm r}/\sqrt{3}$, where $H_{\rm r}$ is the magnetic field equivalent of the universal microwave radiation (van der Laan and Perola 1969). With the present values of $H_{\rm eq}$, however, the electron ages come out not very different from this upper limit.

The electron age and the distance to the nearest lobe head define a velocity v. If the head propagates outwards while simply leaving particles and fields behind, this velocity is that of the head itself. The values are within the velocity range derived by Mackay (1973) from a statistical study of flux densities in double source components. However, is should be noted that the material is not left behind very quietly. The large angles about the leading heads e.g. in 3C223 and 3C452 is clear evidence for velocities perpendicular to the axis which are not much smaller than those of the heads themselves.

Hargrave and Mc Ellin (1975) have pointed out that synchrotron losses will have affected the relativistic electron energy spectrum already at the time the electrons escape from the head, and that the resulting bend in the radio spectrum will migrate towards lower frequencies as the material expands. If the observed spectral index variations are due to this mechanism, then one would expect the spectra to show a bend followed by the 0.5 unit steepening characteristic of a continuous injection situation. The reason for this is that processes in an advancing hot spot occur on spatial and temporal scales much smaller than those relevant to the tail structures. Hence one cannot expect any large scale segregation between electrons which have experienced different values of the synchrotron age factor $\int H^2 \cdot dt$ at the time they escaped from a hot spot. The presence of spectral index variations >0.5 therefore argues against this explanation for the steep spectra.

The values of the various parameters in table 2 do not differ greatly from one source to the other. This is partly a consequence of the usual assumption of equipartition between particles and fields which makes the derived physical parameters less sensitive to differences in observational data. If indeed there are important departures from equipartition, however, then velocities will be higher and ages reduced. The opposite will be true if, as argued by Willis and Strom (1978), the particles continue to be accelerated in the extended emission regions.

5. STRUCTURE OF THE PROJECTED MAGNETIC FIELD

The orientation of the projected magnetic field is clearly related to details in the radio structure (figures 4 and 5). The field runs parallel to boundaries and other elongated features in the total intensity distribution. Deviations from strict axial symmetry are reflected in the field configuration. A field directed away from the head and following the general shape of the associated lower brightness tail is seen in all lobes which contain a bright head close to the outer edge. Further in there is often a region in which the field is oriented perpendicular to the axis of the source.

3C111. Most of the polarized emission in the Nf lobe clearly comes from the bright hot spot itself. The measurements show its *RM* to be low and about the same as that of the rest of the source. The projected field, in contrast to that in the associated tail of emission, is directed nearly at right angles to the main axis of the source. The situation is more complicated in the Sp lobe. Much of the extended low level emission comes from regions not aligned with the main axis (figure 2). The field appears to trace the W edge of the low level extension towards the North. The Sp head is just resolved into a double on the full resolution 4995 MHz polarization map. A comparison between the 1415 and 4995 MHz low resolution maps and the 2695 MHz map by Fomalont (private communication) shows that the *RM* also in this more complex region is small and close to that of the rest of the source. There is little depolarization even at 1415 MHz (figure 3). The calculated directions of the projected magnetic field are shown in figure 5 superimposed on the high resolution maps of Jenkins *et al.* (1977). There is an 18 mJy unresolved polarized feature coincident with the central radio component. It also appears on a similar map prepared from measurements taken at a different date and hence is not likely to be an

© European Southern Observatory • Provided by the NASA Astrophysics Data System

1979A&AS...36..173H

instrumental effect. If its *RM* is not greatly different from that over the rest of the source, it indicates a projected magnetic field approximately in pa 65°. This agrees with the main axis of the source as well as with the orientation of the fine structure observed within the central radio component itself (Pauliny-Toth *et al.* 1976).

3C192. The striking rotation symmetrical "wing" distorsions are reflected also in the projected field configuration. The relation between field orientation and details in the total brightness distribution is especially clear in the Np lobe of this source. The Sf head is resolved by the 4995 MHz beam and has a complex polarization structure. There is no comparable 2695 MHz map of this source, but the *RM* solution together with the absence of depolarization at 1415 MHz in this complex region (figure 3) gives strong evidence that it contains no important polarized region whose *RM* differs greatly from that of the rest of the source. The present measurements of the Np bright region indicate that this contains at least two components with different polarization. The region is barely resolved into what might be a close double by the Cambridge 5 km telescope (Jenkins *et al.* 1977). The polarization of this component cannot be separated from that of nearby regions on the 1415 MHz map.

3C219. Fomalont (1972) noted that the polarization pattern of the Nf lobe was indicative of a circumferential magnetic field and his conclusion is clearly borne out by the present measurements. The field pattern in the Sp lobe is complex but not unlike that expected had there in fact been a bright head at the leading edge. This suggests that the present hot spots and the extended areas represent separate periods of activity. They may also be separated in space, in the direction of the line of sight. The polarized structure in the neighbourhood of the hot spots is complex on a scale equal to or smaller than that corresponding to the 4995 MHz resolution. The jet emanating from the central compact component to the *SW* is strongly polarized with the magnetic field running parallel to the structure. Figure 5 shows the present measurements of the field orientation superimposed on high resolution maps by Turland (1975).

3C223. The projected magnetic field near the Np head closely follows the edges of the structure seen in the high resolution map by Riley and Pooley (1975) (figure 5). The Sf lobe contains no prominent head but the detailed structure of its extreme outer edge with its magnetic field perpendicular to the main axis of the source may indicate the presence of a weak hot spot.

3C315. This source contains no bright heads but, as argued above, the Nf-Sp extensions probably define a recent axis of activity. The source is strongly polarized and the configuration of the projected magnetic field gives a smooth and relaxed impression. In the weak Np extension, which can be traced much further out on the low resolution maps, the polarization rises to 50% or more. There is evidence for a jet some 10 arcsec from the optical position in pa 12°. Possible inner parts of this feature cannot be measured because of confusion with the central radio component. A polarized maximum just N of the optical position may be related to this jet.

3C452. The full resolution 4995 MHz polarization map shows an unresolved feature, surrounded by some complex structure in each main lobe of the source. The 2695 MHz observations by Fomalont (private communication) and the present 4995 MHz observations show that the *RM* in this complex region does not differ much from that of the surrounding parts. The main features of the projected magnetic field in these regions can thus be determined and are shown in figure 5 superimposed on high resolution maps by Riley and Pooley (1975). The field direction is clearly related to edges and elongated features also in these maps. The slight tendency to distortion with rotational symmetry in the extended emission regions of this source is also seen in the configuration of the projected magnetic field.

6. THREE DIMENSIONAL GEOMETRY OF THE MAGNETIC FIELD

The measured polarized radiation is the vector sum of contributions from all radiating regions along the line of sight. Thus, the projected magnetic field may give a false impression of simplicity and, in fact, be only marginally related to the actual three dimensional field geometry. We can extract some information about the field configuration along the line of sight from the measured degree of polarization.

© European Southern Observatory • Provided by the NASA Astrophysics Data System

1979A&AS...36..173H

The projected field in the 3C219 jet runs parallel to the jet itself. On the relativistic beam model this would indicate that the emission does not come from the beam itself but from particles accelerated by dissipation processes at the walls of the beam (Blandford and Rees 1978). The observed degree of polarization, $21 \pm 4\%$, is lower than that from a perfectly aligned field and there are configurations other than the obvious one, e.g. a helically wound field or a radially compressed irregular field that would also be compatible with the measurements. Similar remarks can be made about the field in the nuclear regions of 3C111. The polarization structure near the central component of 3C315 is too complex for a quantitative analysis.

The angular resolution of the present measurements does not permit a detailed study of the polarization in the heads. However, a comparison with high resolution I–Q maps of some of these heads (Turland 1975, Riley and Pooley 1975, Jenkins *et al.* 1977) shows that there must be regions which are polarized to 30% or more within these bright complex regions.

The degree of polarization over the extended emission regions is typically 10-30% at 4995 MHz. This is significantly less than that expected of synchrotron radiation from particles in a perfectly aligned field ($=72\%$ for radiation with a spectral index $\alpha = -0.75$). The moderate depolarization observed as one goes from 4995 MHz to lower frequencies makes it unlikely that internal Faraday rotation can be the cause of the low polarization at 4995 MHz. This should therefore be interpreted in terms of the misalignment of the magnetic fields within that volume of the source which contributes to the measured flux in any one direction. Some misalignment along the line of sight is expected since we see that even the projected field can be quite complex in places, especially close to the heads. In 3C219 and 3C452 one gets the impression that strands of differently oriented fields cross along the line of sight causing "interference minima" in the distribution of the polarized intensity.

Reduction in the degree of polarization by a factor of two will result when there are two or more main contributing regions along the line of sight, the projected field directions of which differ by at least 60°. On such a model, however, one would expect much more fine structure both in the degree of polarization and in the orientation of the projected field over the source. Fine structure is present in some sources, especially close to the leading hot spots. The projected field in the less disturbed parts of many sources, however, appears to be too uniform to be explained by a limited number of very differently oriented strands throughout the source.

A more promising model is one in which the magnetic field is basically irregular. The model calculations by De Young (1977) mentioned in section 3 indicate that the dynamics of this type of source may be dominated by the behaviour of thermal plasma streaming out from the advancing head. Magnetic fields carried out with the thermal plasma are then likely to be highly irregular in nature. Shear and/or compression will make the field anisotropic. Polarized emission will then be observed from regions of shear or compression and only in very extreme situations would one expect to approach the degree of polarization expected from a perfectly aligned field. In the extended regions as well as in the hot spots and their complex neighbourhood one would naturally expect both shear and compression to work in such a way that one observes a projected magnetic field aligned parallel to major structural details. The emission from localized regions of compression should be both enhanced and highly polarized. The full resolution 4995 MHz maps contain many features that can be interpreted as due to localized regions of compression.

A basically irregular field will serve to slow down the diffusion of charged particles, and relativistic electrons of different age can be kept separate while following the thermal plasma along with the associated magnetic fields. The parameters in table 2 are derived on the assumption that there has been no significant mixing of relativistic electrons of different age.

7. FARADAY ROTATION AND DEPOLARIZATION

The observed Faraday rotation may be intrinsic to the source or it may be due mainly to the passage of the radio waves through the interstellar medium of the Galaxy. Differences in the rotation measure

© European Southern Observatory • Provided by the NASA Astrophysics Data System

1979A&AS...36..173H

over individual sources, however, are probably due to the conditions in or near the source itself (Strom 1973). Furthermore, in 3C192 and 3C452, there appears to be some relation between the distribution of rotation measure and the distribution of polarized intensity.

Areas with significantly different *RM* have been found in 3C111, 3C192 and 3C452. The 3C111 Sp head and the main part of the associated diffuse extension towards the *NW* have a $RM = -15 \pm 3$ rad m^{-2} while that of the remaining portions of the source including the Nf bright head is -3 ± 4 rad m^{-2}. The depolarization in the central parts of the 3C192 profile may be due to the overlap, at this low resolution, of two regions with the measured *RM* difference and different polarization position angles. 3C452 displays large variations both in rotation measure and depolarization.

All sources, with the exception of 3C452, have low median rotation measures compatible with an origin in the Galaxy. The intrinsic rotation measures of these sources must be small. 3C452 has a large negative median rotation measure, -280 rad m^{-2}. According to Kronberg and Simard-Normandin (1976) the magnitude of the galactic component is seldom more than 60 rad m^{-2} at latitudes $|b| > 10°$. However, 3C452 is not far from this limit ($\ell = 98°$, $b = -17°$) and is situated within a band of latitudes which abounds in sources with exceptionally large negative rotation measures. Hence it seems that the galactic contribution can account for a major portion of the 3C452 median rotation measure. Such an interpretation is supported by the observation that the *RM* in the bright hot spots is not greatly different from that of neighbouring regions.

3C452 displays a striking symmetry in its general structure, its spectral index distribution and also its projected magnetic field configuration but the two halves of the source are less similar in certain polarization characteristics. The degree of polarization at 4995 MHz is comparable in the two main lobes but, as previously noted by Riley and Branson (1973), there is substantial depolarization in the Sp but not in the Nf lobe (figure 3). The full resolution 4995 MHz maps reveal a complex polarization structure in the Sp lobe and there may be further structural detail not resolved by the 7×11 arcsec beam. The polarized structure in the Nf lobe, however, appears to be resolved: its general appearence does not change a great deal when the map is smoothed to half the angular resolution. Hence it is possible that the depolarization in the Sp lobe is wholly or partly a resolution effect. This is not unreasonable since the low resolution maps reveal *RM* differences within this lobe which are barely resolved and about half as large as those required for effective depolarization at 1415 MHz. The *RM* over the Nf lobe on the other hand changes less drastically from one beam area to the next.

The symmetry in most other observational parameters makes it unlikely that the polarization asymmetry reflects some fundamental difference in the physics of the two lobes. Total intensity, spectral index and the direction of the projected magnetic field depend upon simple integrals along the line of sight and hence symmetry is preserved also when the source is oriented at an angle to the plane of the sky. The degree of polarization and the position angle of the electric vector on the other hand depend upon the exact sequence of radiating and rotating regions along the line of sight. This will in general be different along corresponding lines of sight in the lobes pointing towards and away from the observer. The depolarization asymmetry is probably a result of 3C452 being inclined to the plane of the sky. However, it is not immediately obvious which of the two lobes is the closest; the answer depends upon which models is adopted for the source and its immediate neighbourhood.

The depolarization and the variations in the *RM* over individual sources is evidence for magnetized thermal plasma in or near the radio emitting regions. The *RM* and depolarization measurements can in principle be used to derive the thermal electron density, but only if the distribution in space of magnetic fields, relativistic electrons and thermal electrons are all known. Lacking such a detailed model one can estimate a "probable" order of magnitude by making the simplifying assumptions that the relativistic electrons and the thermal electrons are well mixed and the magnetic field close to its equipartition value. Such an approach leads to values or, in areas with no measurable depolarization, upper limits, of $(1\text{-}2) \cdot 10^{-4} \cdot N^{1/2}$ cm^{-3} for the extended emission regions. N is here the number of independent rotational elements along the line of sight. If, as argued above, the magnetic field has an irregular structure, then N is large and the thermal

© European Southern Observatory • Provided by the NASA Astrophysics Data System

1979A&AS...36..173H

electron density can be much higher than 10^{-4} cm^{-3}. It should be kept in mind that this number depends upon several assumptions about the detailed conditions in the source and its vicinity, some of which may not be correct.

8. CONCLUSIONS

The six sources display to a varying extent the normal linear double structure. The remarkable double arc configuration of 3C315 is seen to be an extreme case of a rotation symmetrical distorsion also present in 3C192 and, to a lesser extent, in 3C452. In typical radio lobes where the brightness of the tail decreases continuously away from the associated head, the spectrum steepens inwards along the tail. Interpreted as an effect of energy losses of the radiating electrons this points at velocities for the heads of 0.02-0.08 c. Equipartition magnetic field strengths in the extended emission regions are in the range 4 to 8 μ Gauss.

The observations have revealed an almost perfect relation between the projected magnetic field and the total brightness distribution. The field runs parallel to edges and other elongated features. It is suggested that this relation as well as the low degree of polarization (relative that expected of radiation from a perfectly aligned field) can be understood if the magnetic field is basically irregular. Linear polarization is then observed from regions where shear and/or compression has made the field anisotropic. The presence of localized regions of enhanced strongly polarized emission is evidence for compression.

All six sources contain a central unresolved radio component coincident with the parent galaxy. There is evidence that the field in jets associated with such components is aligned parallel to the jets themselves, possibly a consequence of interaction between a relativistic beam and the medium through which it travels.

ACKNOWLEDGEMENTS

I am greatly indebted to E.B. Fomalont for allowing me to use his unpublished 2695 MHz polarization observations. The maps of figure 5 have been reproduced with the kind permission of the authors and the Royal Astronomical Society. The work has been supported by the Swedish Natural Science Research Council (N.F.R.). The Westerbork Radio Observatory is operated by the Netherlands Organization for the Advancement of Pure Research (Z.W.O.).

REFERENCES

Blandford, R.D. and Rees, M.J.: 1978, Proceedings of the Copenhagen Symposium on "Active Nuclei", 1977, *Phys. Scr.* **17**, 265.
Burch, S.F.: 1977, *Monthly Notices Roy. Astron. Soc.* **180**, 623.
Burn, B.J.: 1966, *Monthly Notices Roy. Astron. Soc.* **133**, 67.
De Young, D.S.: 1977, *Astrophys. J.* **211**, 329.
Fomalont, E.B.: 1972, *Astrophys. Lett.* **12**, 187.
Hargrave, P.J. and McEllin, M.: 1975, *Monthly Notices Roy. Astron. Soc.* **173**, 37.
Harris, A.: 1974, *Monthly Notices Roy. Astron. Soc.* **166**, 449.
Haves, P.: 1975, *Monthly Notices Roy. Astron. Soc.* **173**, 553.
Högbom, J.A. and Brouw, W.N.: 1974, *Astron. Astrophys.* **33**, 289.
Högbom, J.A.: 1974, *Astron. Astrophys. Suppl.* **15**, 417.
Högbom, J.A. and Carlsson, I.: 1974, *Astron. Astrophys.* **34**, 341.
Jenkins, C.J., Pooley, G.G. and Riley, J.M.: 1977, *Mem. Roy. Astron. Soc.* **84**, 61.
Kellermann, K.I., Pauliny-Toth, I.I.K. and Williams, P.J.S.: 1969, *Astrophys. J.* **157**, 1.
Kronberg, P.P. and Simard-Normandin, M.: 1976, *Nature* **263**, 653.
Longair, M.S. and Gunn, J.E.: 1975, *Monthly Notices Roy. Astron. Soc.* **170**, 121.
Mackay, C.D.: 1973, *Monthly Notices Roy. Astron. Soc.* **162**, 1.
Matthews, T.A., Morgan, W.W. and Schmidt, M.: 1964, *Astrophys. J.* **140**, 35.
Miley, G.K., Perola, G.C., van der Kruit, P.C. and van der Laan, H.: 1972, *Nature* **237**, 269.

© European Southern Observatory • Provided by the NASA Astrophysics Data System

1979A&AS...36..173H

Miley, G.K.: 1976, in G. Setti (ed.), The Physics of Non-Thermal Radio Sources, Proceedings of the NATO Advanced Study Institute, Urbino 1975, p. 1.
Northover, K.J.E.: 1976, *Monthly Notices Roy. Astron. Soc.* **177**, 307.
Pauliny-Toth, I.I.K., Preuss, E., Witzel, A., Kellermann, K.I. and Shaffer, D.B.: 1976, *Astron. Astrophys.* **52**, 471.
Rayburn, D.R.: 1977, *Monthly Notices Roy. Astron. Soc.* **179**, 603.
Riley, J.M. and Branson, N.J.B.A.: 1973, *Monthly Notices Roy. Astron. Soc.* **164**, 271.
Riley, J.M. and Pooley, G.G.: 1975, *Mem. Roy. Astron. Soc.* **80**, 105.
Sandage, A.: 1966, *Astrophys. J.* **145**, 1.
Sargent, W.L.W.: 1977, *Astrophys. J.* **212**, L105.
Scheuer, P.A.G.: 1974, *Monthly Notices Roy. Astron. Soc.* **166**, 513.
Schmidt, M.: 1965, *Astrophys. J.* **141**, 1.
Strom, R.G.: 1973, *Astron. Astrophys.* **25**, 303.
Turland, B.D.: 1975, *Monthly Notices Roy. Astron. Soc.* **172**, 181.
van der Laan, H. and Perola, G.C.: 1969, *Astron. Astrophys.* **3**, 468.
Weiler, K.W.: 1973, *Astron. Astrophys.* **26**, 403.
Willis, A.G. and Strom, R.G.: 1978, *Astron. Astrophys.* **62**, 375.
Wyndham, J.D.: 1966, *Astrophys. J.* **144**, 459.

J.A. Högbom

Stockholm Observatory
S–13300 Saltsjöbaden (Sweden)

© European Southern Observatory • Provided by the NASA Astrophysics Data System

1979A&AS...36..173H

Table 1 Optical data and observations of the central unresolved radio components.

Source	Ident.	z	D Mpc	Scale kpc/″	b	α_r(h,m,s) ± $\alpha_{opt}-\alpha_r$ δ_r(°,′,″) ± $\delta_{opt}-\delta_r$	S(1415)± mJy	S(4995)± mJy
3C111	18^m	.0488	198	0.87	- 9	04 15 00.61 .05 .00 37 54 19.2 .9 -.2	1100 100 (1971.4)	1450 30 (1975.1)
3C192	15^m E0	.0597	242	1.05	+26	08 02 35.35 .1 +.06 24 18 24.7 2. +2.2	<40 (1971.4)	8 4 (1973.0)
3C219	18^m cD5	.1745	726	2.55	+45	09 17 50.66 .05 -.01 45 51 43.3 .8 +.6	60 30 (1971.4)	48 4 (1975.1)
3C223	17^m E2	.1367	564	2.12	+49	09 36 50.95 .1 -.13 36 07 36.7 2. -1.7	< 30 (1971.4)	8 3 (1975.1)
3C315	17^m DE2	.1086	446	1.76	+58	15 11 30.81 .03 -.09 26 18 40.5 .8 -1.7	390 50 (1971.4)	150 10 (1973.0)
3C452	16^m ED1	.0820	335	1.39	-17	22 43 32.86 .05 -.07	140 70 (1971.4)	150 8 (1973.0)

Identifications and redshifts are by Longair and Gunn (1975), Matthews *et al.* (1964), Sandage (1966), Sargent (1977), Schmidt (1965) and Wyndham (1966). The optical positions are taken from Jenkins *et al.* (1977), Riley and Pooley (1975) and Turland (1975). The 1415 MHz flux densities are derived from the measurements of Högbom and Carlsson (1974), see text. Luminosity distances correspond to a Hubble constant of 75 kms^{-1} Mpc^{-1} and a deceleration parameter $q=0.5$.

Table 2 Physical parameters at selected locations in the extended regions of emission

Source	loc.	α_h	$(\alpha-\alpha_h)$ ±	B(4995) mJy/arcsec^2	L kpc	H_{eq} μG	u_{min} 10^{-12} erg/cm^3	t_{eq} 10^6y	v/c	T 10^6y
3C111	A	-.74	-.06 .08	.42	20	9	7	< 5	> .02	< 13
	B	-.74	-.10 .08	.28	30	7	5	≃ 5	≃ .04	
	C	-.76	+.01 .2	.09	65	4	1.5	< 12	> .04	
3C192	A	-.68	+.03 .08	.34	30	7	4	< 4	> .03	< 10
	B	-.68	-.16 .2	.07	35	5	2	< 15	> .03	
3C219	A	-.82	-.28 .08	.30	40	7	5	7	.03	15
	B	-.82	-.28 .08	.14	50	7	5	7	.03	
3C223	A	-.80	+.05 .08	.22	60	6	3	< 2	> .1	13
	B	-.80	-.20 .08	.07	60	5	2	8	.08	
3C315	A	-.79	-.11 .05	.22	40	7	5	5	.06	10
	B	-.79	-.26 .1	.09	50	6	3	9	.03	
3C452	A	-.72	-.08 .05	.35	60	6	4	5	.03	18
	B	-.72	-.48 .08	.18	60	6	4	12	.03	
	C	-.74	-.53 .08	.18	60	7	4	12	.04	

The selected locations are marked on the total intensity maps of figure 1. The calculations have been made assuming a Hubble constant of 75 kms^{-1} Mpc^{-1} and a deceleration parameter $q=0.5$.

α_h(1415,4995), spectral index of the head region in the same lobe, derived from the $22\times22/\sin\delta$ arcsec resolution maps. There are no radio heads in 3C315 and α_h has been set equal to the integrated low frequency spectral index between 38 and 750 MHz from Kellermann *et al.* (1969).

α(1415,4995), spectral index at the selected location derived from the $22\times22/\sin\delta$ arcsec resolution maps.

B(4995), radio brightness. The 4995 MHz structure is well resolved at all the selected locations and the brightness is taken directly from the maps. In some weak regions, the smoothed versions of these maps have been used.

L, estimated line of sight path through the source at the selected location.

H_{eq}, magnetic field corresponding to the minimum energy density situation (≃ equipartition field).

u_{min}, minimum total energy density in relativistic particles and magnetic fields, assuming that observed differences between α(1415,4995) and α_h(1415,4995) are caused by energy losses by synchrotron emission and by inverse Compton encounters with microwave background photons, see text.

t_{eq}, age of the relativistic electrons assuming they have spent all the time in a field H_{eq}.

v, the velocity defined by the age t_{eq} and the projected distance to the closest head or, for 3C315, to the central component.

T, age of the source assuming that the heads have travelled with a constant velocity v from the parent galaxy to their present positions.

© European Southern Observatory • Provided by the NASA Astrophysics Data System

© European Southern Observatory • Provided by the NASA Astrophysics Data System

1979A&AS...36..173H

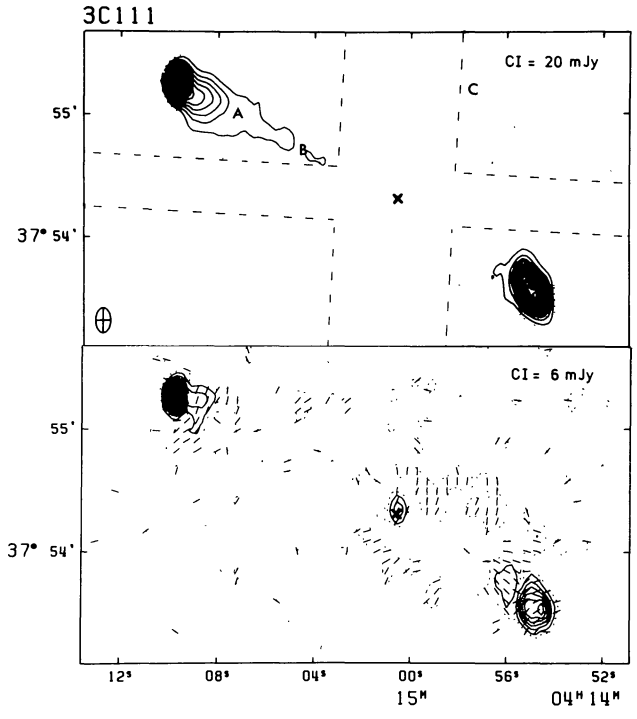

3C111: due to some instrumental malfunction, the weak regions in parts of the *I* map are visibly affected by sidelobes from the very intense central component (table 1). These regions have been left blank on the *I* map. The polarization map is less affected and the 18 mJy maximum at the optical position is probably genuine. The Nf head reaches a maximum level of 774 mJy/beam on the *I* map and 136 mJy/beam in p.a. 55° on the polarization map. In the Sp head the *I* map reaches 363 mJy/beam.

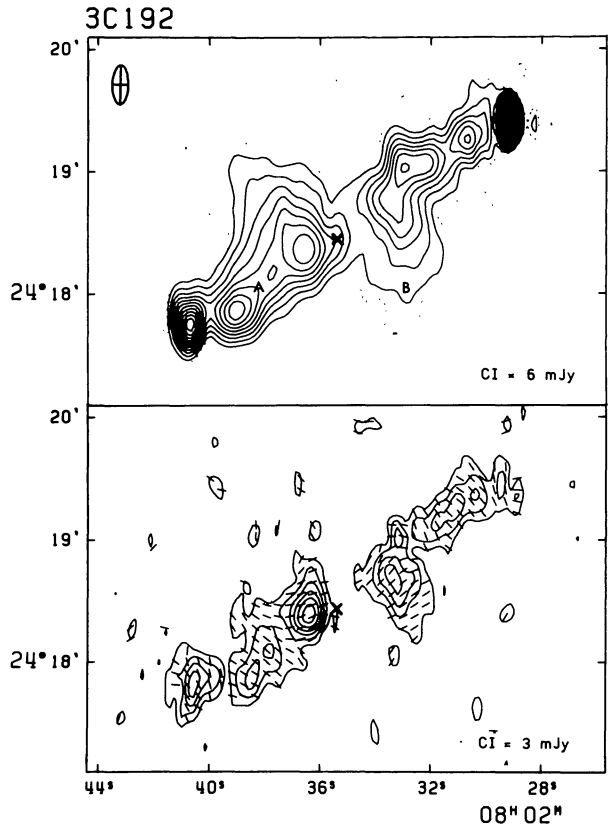

3C192: The maximum levels in the Sf and Np heads are, respectively, 75 and 164 mJy/beam.

Figure 1 The 4995 MHz total brightness distribution (Stokes parameter I) and linearly polarized brightness distribution (Stokes parameter $(Q^2+U^2)^{1/2}$) for the six sources. The direction of the electric vector is indicated by the short lines on the polarization maps and the half power contour of the synthesized beam is shown in one corner of the total intensity map. The contour interval expressed in mJy is given with each map; a point source with this flux density will cause a peak deflection of one contour interval. A dashed contour, when present, is drawn at the level of one half contour interval. Zero contours, as well as the occasional negative contour on the *I* maps have been omitted for clarity. Over extended regions a level of 1 mJy corresponds to a brightness temperature of 1.3 sin δ K. A cross marks the optical position of the parent galaxy. Locations marked A, B, C on the total intensity maps are those referred to in table 2.

1979A&AS...36..173H

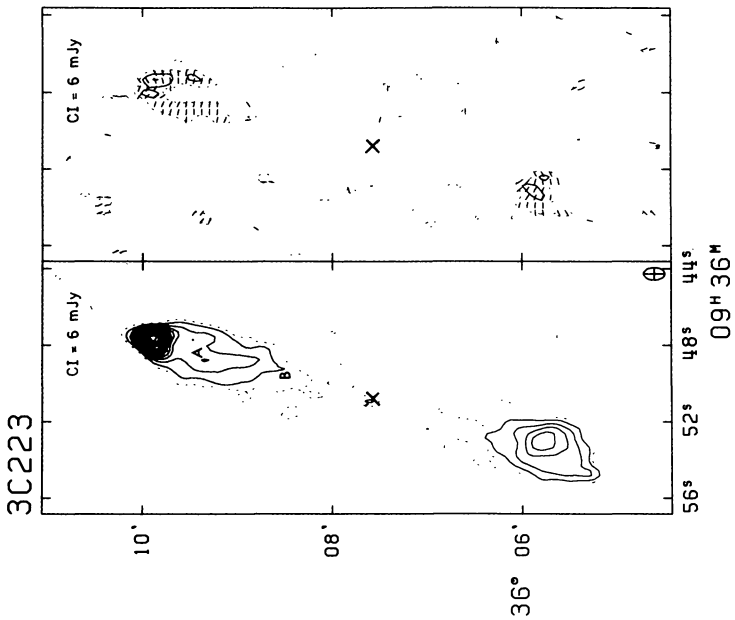

3C223: The maximum level in the Np head is 88 mJy/beam.

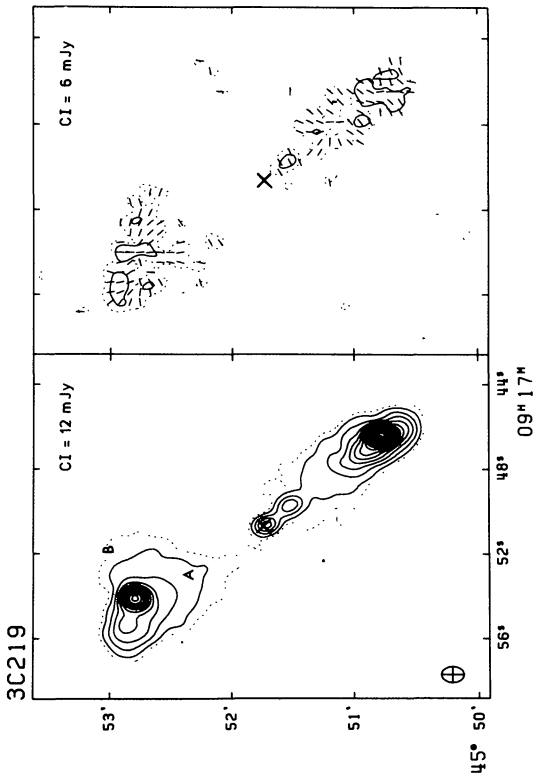

3C219: The bright regions in the Nf and Sp lobes reach, respectively, 131 and 210 mJy/beam.

© European Southern Observatory • Provided by the NASA Astrophysics Data System

1979A&AS...36..173H

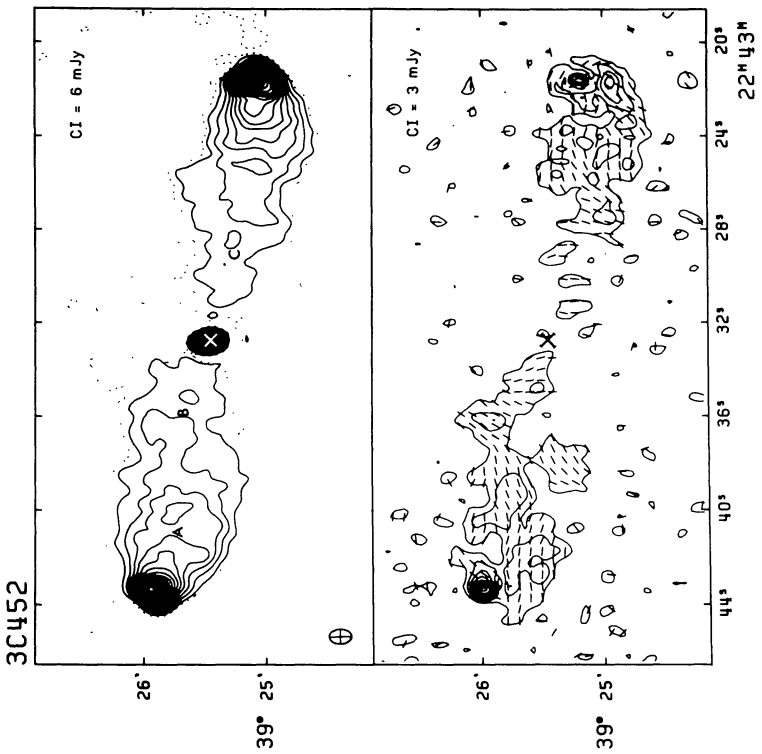

3C542: The maximum levels in the Nf and Sp heads are, respectively, 117 and 112 mJy/beam. The *I* maxima coincide with unresolved polarization maxima of 25 mJy/beam in p.a. 160° and 15 mJy/beam in p.a. 30°. A detailed comparison with the high resolution maps from Cambridge (figure 5) shows that the brightest spots in these areas are 40-50% polarized.

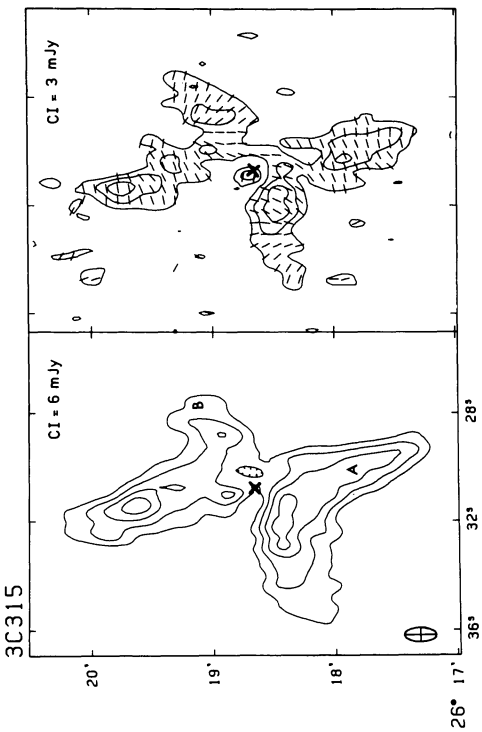

3C315: A 150 mJy unresolved component associated with the parent galaxy (table 1) has been subtracted from the *I* map in order to show more clearly the shape of the extended emission regions.

© European Southern Observatory • Provided by the NASA Astrophysics Data System

1979A&AS...36..173H

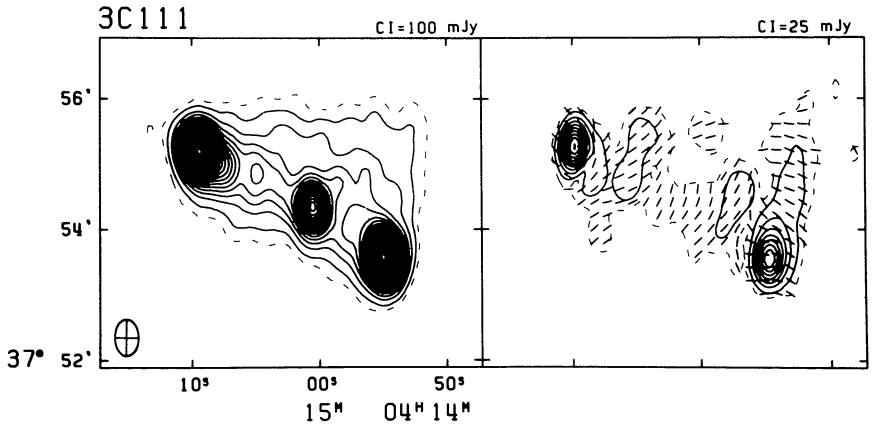

Figure 2 Maps of the total intensity and the polarization of 3C111 at 1415 MHz, prepared with a 22 × 36 arcsec gaussian beam.

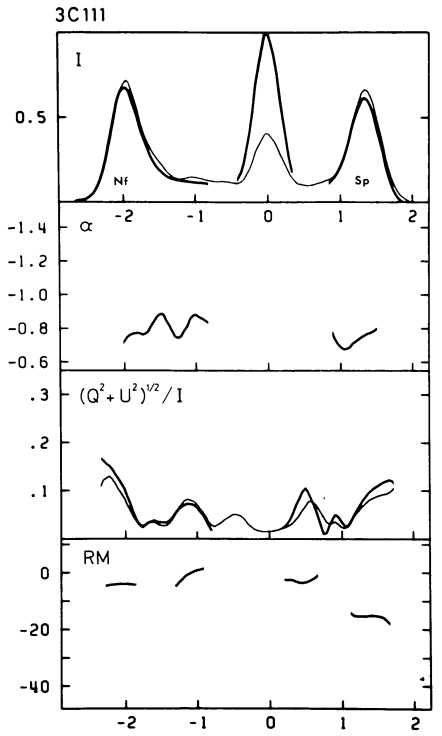

3C111: The 4995 MHz sidelobe problems (see figure 1) make the spectral index profile less accurate than for the other sources. The main features of the polarization and rotation measure profiles should be reliable.

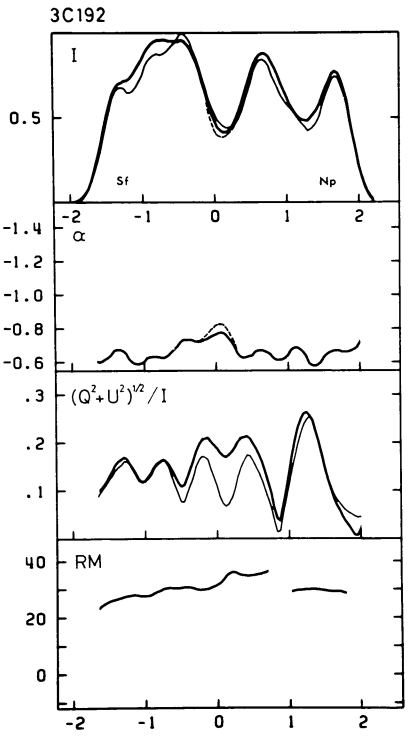

3C192: The spectral index is remarkably constant apart from a slight steepening of the spectrum in the immediate vicinity of the parent galaxy.

Figure 3 Total intensity, spectral index, degree of polarization and rotation measure calculated from 22 × 22/sin δ arcsec resolution maps at 1415 and 4995 MHz. The parameters are plotted along two connecting straight lines, one through the W maximum to the central radio component and the other from there through the E maximum. The horizontal scale is expressed in arcmin from the central radio component. Thin lines and heavy lines in the I and the $(Q^2+U^2)^{1/2}/I$ profiles refer to the 1415 and 4995 MHz measurements respectively. The I profiles are scaled in such a way that they overlap for a spectral index $\alpha(1415,4995)=-0.7$. The nature of the plotted parameters makes it difficult to specify errors over these profiles. Spectral index, degree of polarization and rotation measure depend upon measurements whose relative (but not absolute) accuracy varies over the profiles. They have not been continued into regions where they are obviously unreliable. Dashed lines indicate the shape of the profiles after subtracting the influence of the central compact radio component (see text).

© European Southern Observatory • Provided by the NASA Astrophysics Data System

1979A&AS...36..173H

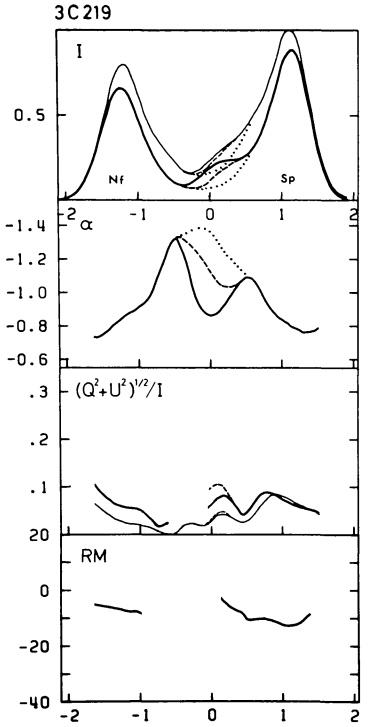

3C219: The dotted lines in the *I* and α profiles are obtained after the subtraction of both the central component and the jet seen on the full resolution 4995 MHz map, assuming the latter to have a spectral index of −0.7. The spectrum becomes progressively steeper all the way to the zero (central compact component) position if the spectral index of the jet is $\alpha > -1.1$. The maximum in the degree of polarization at +0.2 arcmin from the centre is almost entirely due to the jet. The apparent depolarization is caused by the steep spectrum of the radio tail and is not evidence for depolarization in the jet itself.

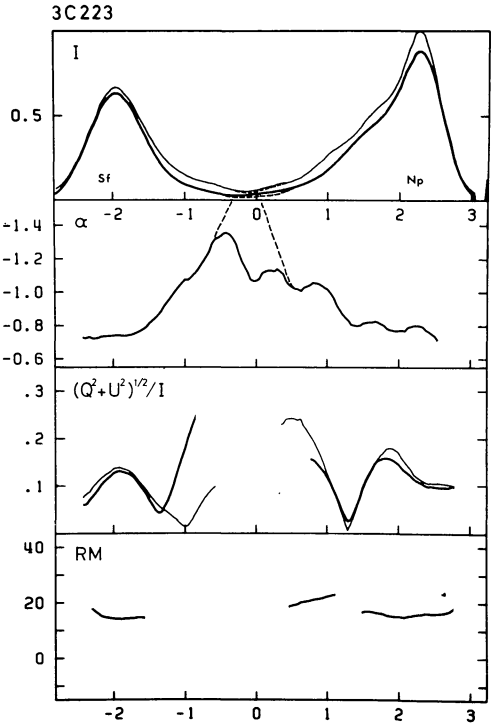

3C223: Apart from the weak central component, the central parts of the 4995 MHz *I* profile are not significantly different from zero. At 1415 MHz, however, emission is clearly present.

© European Southern Observatory • Provided by the NASA Astrophysics Data System

1979A&AS...36..173H

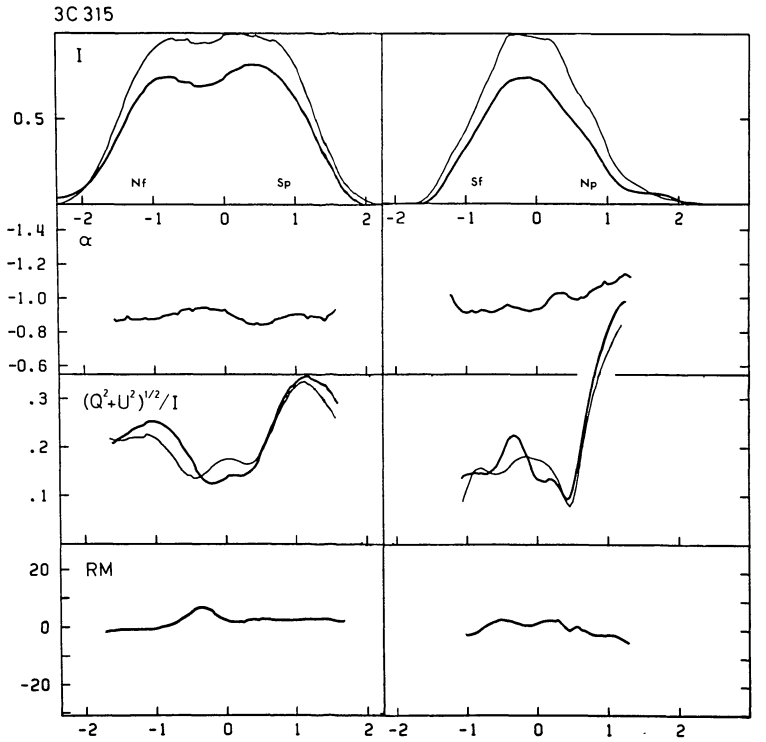

3C315: Two profiles are shown, the first through the main Nf-Sp extensions and the second through the Sf-Np extensions. A central point source 155 mJy at 4995 MHz and 390 mJy at 1415 MHz has been subtracted from all profiles. There are then no significant variations of the rotation measure over the source and no significant depolarization. The spectrum steepens and the degree of polarization increases to about 50% in the faint outer parts of the Np extension.

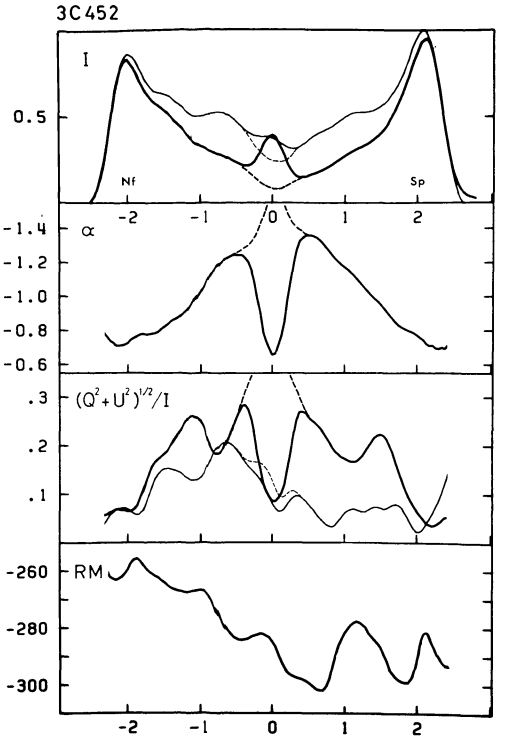

3C452: The S/N and the general quality of these measurements are very good and the various parameters well defined over the full profile. In particular note the inward steepening of the spectrum, the symmetric polarization profile at 4995, the marked depolarization of the Sp (but not the Nf) lobe and the large variations in the rotation measure.

© European Southern Observatory • Provided by the NASA Astrophysics Data System

1979A&AS...36..173H

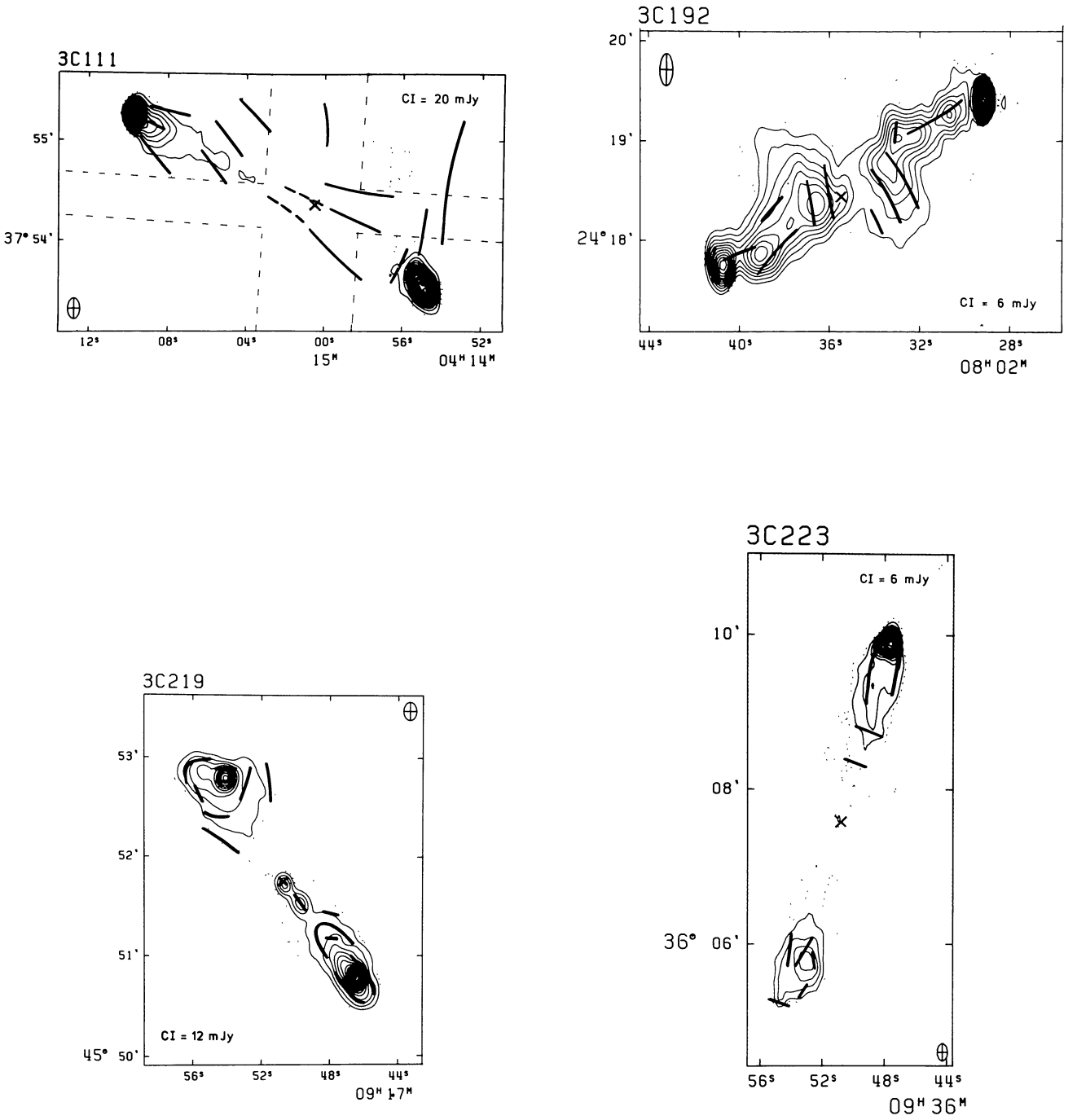

Figure 4 Main features of the projected magnetic field in the extended regions of emission (heavy lines) superimposed on maps of the total intensity. Continuous lines have been drawn where there are no obvious transitions between regions with different properties. The orientation of the field in faint extended regions has been determined from smoothed versions of the 4995 MHz polarization maps. The detailed structure of the field in some bright radio heads is shown in figure 5.

© European Southern Observatory • Provided by the NASA Astrophysics Data System

1979A&AS...36..173H

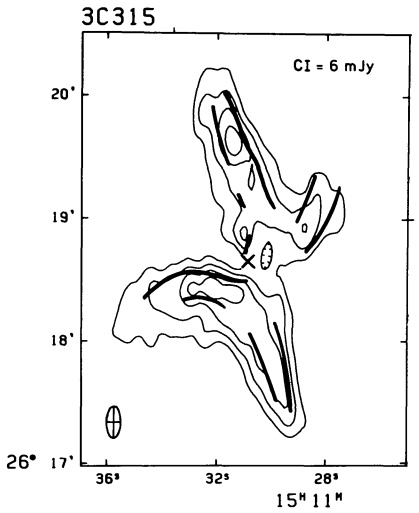

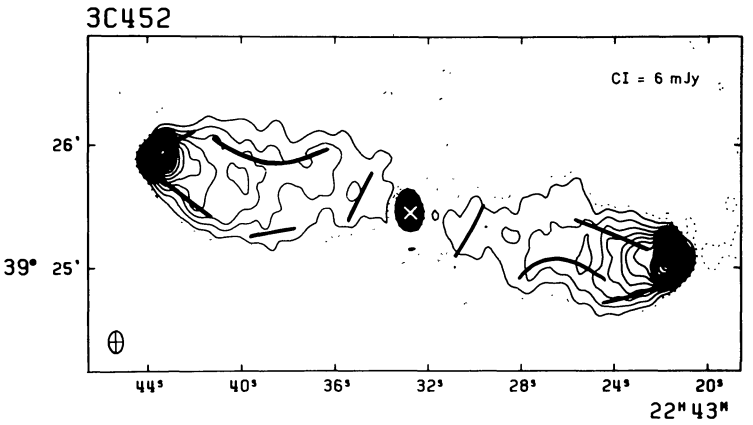

Figure 4 *(continued)*

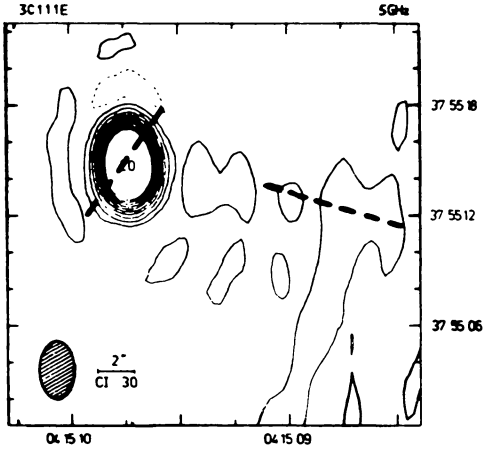

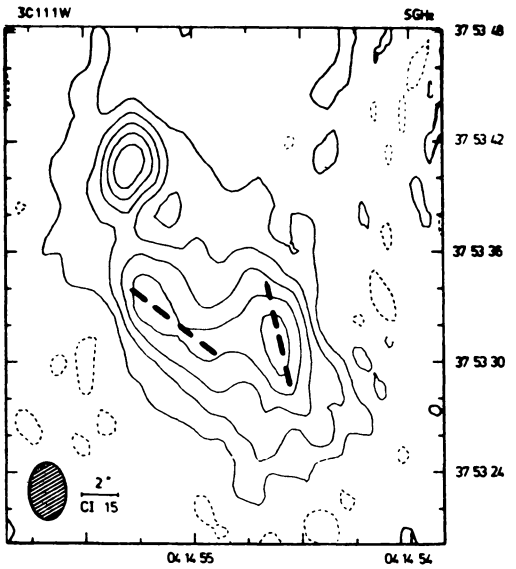

3C111: Maps by Jenkins *et al.* (1977). Nf head (left) and Sp head (right).

Figure 5 The orientation of the projected magnetic field in some bright regions (dashed heavy lines) superimposed on high resolution $(I-Q)$ maps from the Cambridge 5 km telescope (reproduced with permission).

© European Southern Observatory • Provided by the NASA Astrophysics Data System

1979A&AS...36..173H

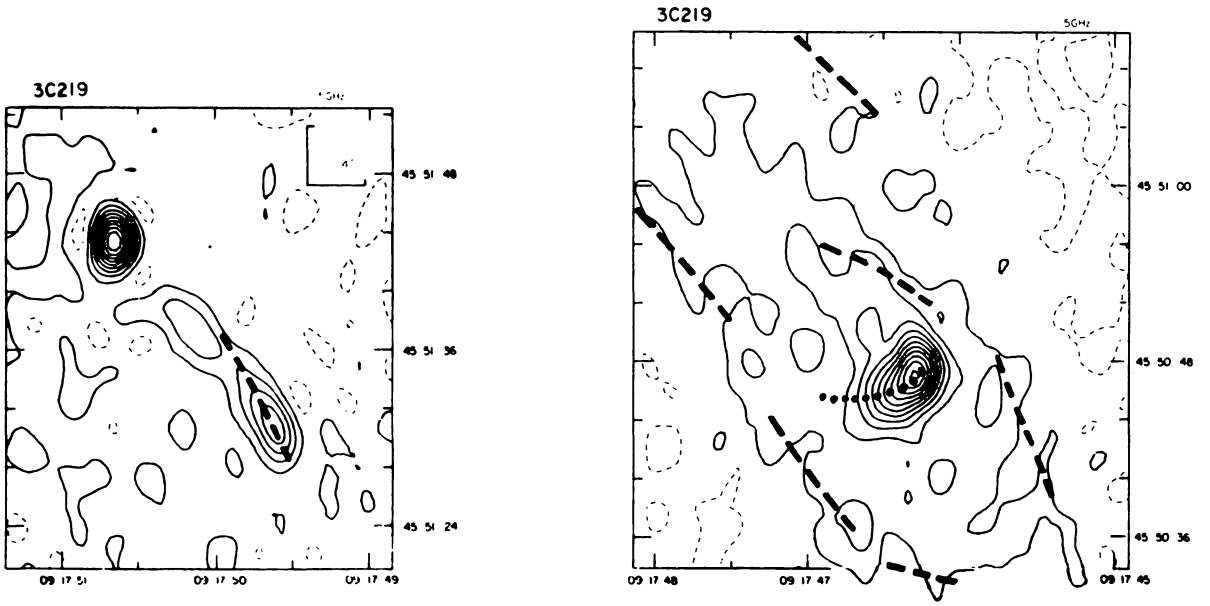

3C219: Maps by Turland (1975). Central compact component with jet (left) and Sp head (right). The dotted line refers to a region which is too confused on the present measurements for the field direction to be sorted out properly.

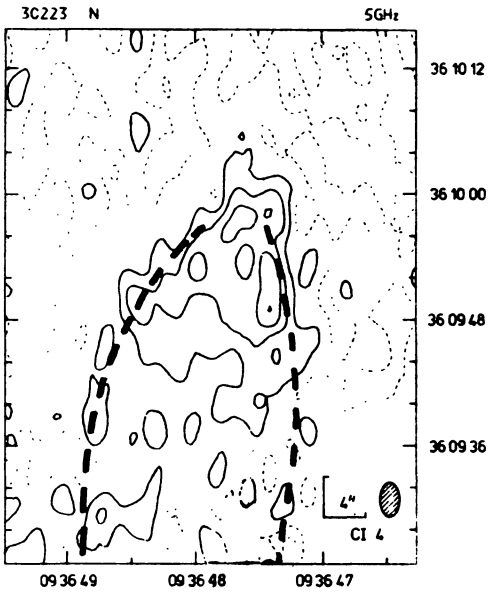

3C223: Np head, map by Riley and Pooley (1975).

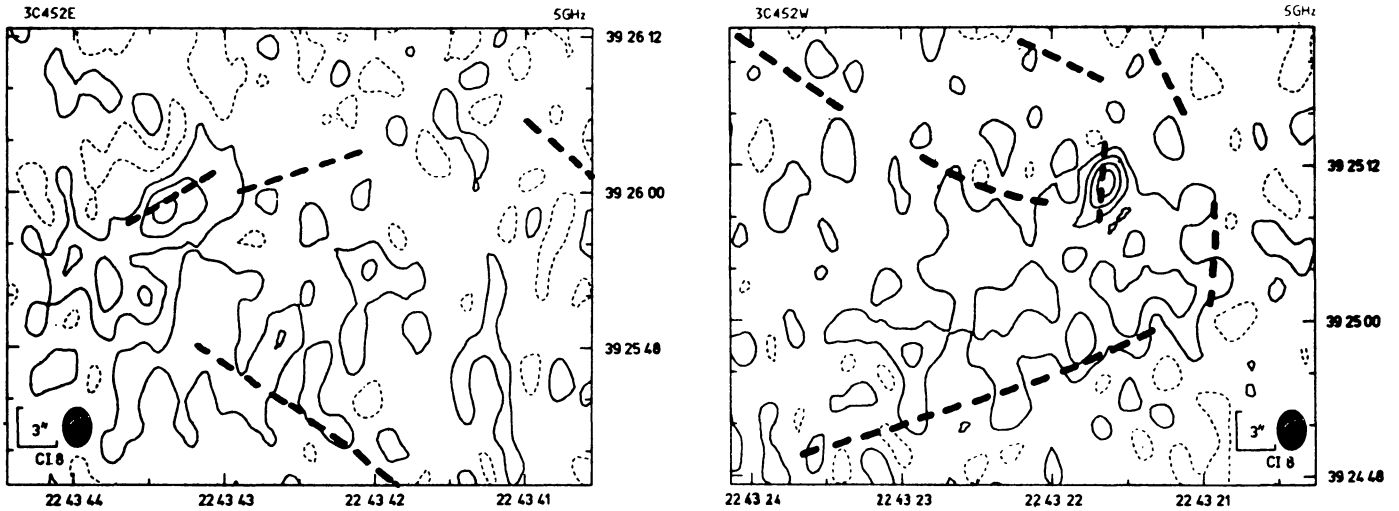

3C452: maps by Riley and Pooley (1975). Nf head (left) and Sp head (right).

Figure 5 *(continued)*

© European Southern Observatory • Provided by the NASA Astrophysics Data System